ChemComm

COMMUNICATION

View Article Online
View Journal | View Issue



Cite this: *Chem. Commun.*, 2020, **56**, 3449

Received 20th December 2019,
Accepted 17th February 2020

DOI: 10.1039/c9cc09884d

rsc.li/chemcomm

# Pressure-induced inclusion of neon in the crystal structure of a molecular $Cu_2$(pacman) complex at 4.67 GPa†

Nico Giordano, ‡[ab] Christine M. Beavers, §[bc] Konstantin V. Kamenev, [d] Jason B. Love, [a] James R. Pankhurst, [a] Simon J. Teat [b] and Simon Parsons *[a]

**Crystals of a Cu complex of the macrocyclic Schiff-base calixpyrrole or 'Pacman' ligand, $Cu_2$(L), do not contain any solvent-accessible void space at ambient pressure, but adsorb neon at 4.67 GPa, forming $Cu_2$(L)·3.5Ne.**

Although avoidance of very short intermolecular interactions is sometimes the dominating driving force for high-pressure phase transitions, the most important factor is usually the pressure × volume contribution to the lattice free energy, a consequence of the need to fill space efficiently. For example, the organic compound methyl 2-(carbazol-9-yl)benzoate is unusual in crystallising with eight molecules in the crystallographic asymmetric unit ($Z'$ = 8), but at 5.3 GPa (~53 000 atm) it transforms to a $Z'$ = 2 phase with a volume reduction of 7 Å$^3$ per molecule.[1] The contribution of the *PV* term to the transition is 23 kJ mol$^{-1}$. This is a large figure in the context of, for example, polymorph energy differences (estimates are typically <2 or 4 kJ mol$^{-1}$),[2,3] showing that quite substantial deformations are possible provided they lead to more efficient occupation of space. Most of the deformation is accommodated in the intermolecular interactions, but intramolecular conformational flexibility can also play an important role.

In a high pressure experiment a crystal is placed in a diamond anvil cell (DAC) along with a fluid which maintains hydrostatic conditions. A popular choice is a 4 : 1 mixture of methanol and ethanol, though many others are available.[4] Hydrostatic media usually act to compress the sample, but the medium can also sometimes penetrate the sample forming a host–guest complex or cocrystal which minimises the total volume of the sample plus the medium. This is seen in framework materials such as ZIF-8, where initial compression leads to solvent (in this case methanol) ingress leading to an expansion in the unit cell volume.[5] The effect can be used to locate all potential guest sites in a framework by promoting complete occupation of all of them, as was seen the metal organic framework $Sc_2(BDC)_3$ with $CO_2$ and $CH_4$ (BDC = 1,4-benzenedicarboxylate).[6] Noble gases are also used as hydrostatic media, and up-take of neon has been observed in nickel and iron-based porous framework materials.[7,8] It has also been recently seen in initially non-porous 4-hydroxycyanobenzene, where helium becomes incorporated at 2.4 GPa,[9] the formation of $As_2O_3$·2He at 3 GPa[10–12] and with Ne above 0.69 GPa and Ar above 0.18 GPa in methylammonium lead triiodide.[13]

In this report we show that adsorption of neon can be induced in crystals of a flexible macrocyclic Cu 'pacman' complex [$Cu_2$(L), Fig. 1][14] by exploiting the ability of high pressure to perturb its conformation.[15–18] Pacman complexes exhibit catalytic activity which relies on the flexibility of the ligand to enable small-molecule inclusion in the cleft. For example, the active dicobalt pacman complex contains $O_2$ coordinated within the cleft of the pacman ligand forming the intermediate in the reduction of dioxygen to water.[19]

The most obvious hydrostatic medium to use for this study would have been dioxygen itself, but as a liquid at high pressure this is extremely reactive, and rapidly oxidises the complex. We turned instead to neon, which is inert, and is hydrostatic to 15 GPa.[4] The sample was loaded into a diamond anvil cell with ruby as a pressure marker and a rhenium gasket. The cell was gas-loaded with Ne and diffraction data were collected to 8.13 GPa on Beamline 12.2.2 at the Advanced Light Source;[20] further experimental and analysis details are available in the ESI.†

[a] *EaStCHEM School of Chemistry and Centre for Science at Extreme Conditions, The University of Edinburgh, King's Buildings, W. Mains Rd, Edinburgh, UK EH9 3FJ, UK. E-mail: simon.parsons@ed.ac.uk*
[b] *Advanced Light Source, Lawrence Berkeley National Laboratory, 1 Cyclotron Road, Berkeley, CA 94720-8229, USA*
[c] *Department of Earth & Planetary Sciences, University of California, Santa Cruz, 1156 High Street, Santa Cruz, CA 95064, USA*
[d] *Centre for Science at Extreme Conditions and School of Engineering, The University of Edinburgh, King's Buildings, West Mains Road, Edinburgh, Scotland, EH9 3FD, UK*

† Electronic supplementary information (ESI) available: Experimental procedures, further figures and table, animations showing the path of compression. CCDC 1972723–1972725 and 1972728–1972733. For ESI and crystallographic data in CIF or other electronic format see DOI: 10.1039/c9cc09884d

‡ Present address: PETRA-III, Notkestraße 85, 22607 Hamburg, Germany.
§ Present address: Diamond Light Source, STFC Rutherford Appleton Laboratory, Harwell Science and Innovation Campus, Harwell Oxford, Didcot, OX11 0QX, UK.

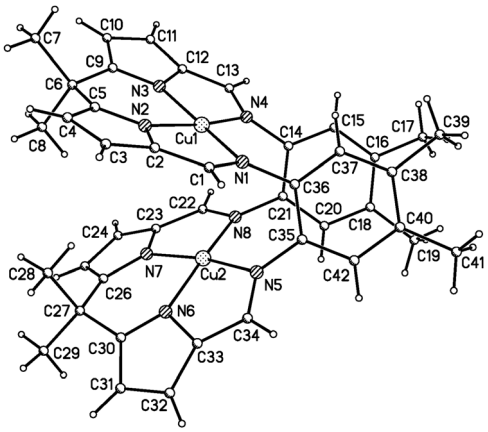


Fig. 1 The Cu-pacman complex $Cu_2(L)$ at ambient conditions and the associated atom labelling.

The crystal structure of $Cu_2(L)$ at ambient pressure and 298 K contains layers of molecules oriented with their longest inertial axes perpendicular to the layer (Fig. 2). Within the layer each molecule is surrounded by six others (Fig. 2a) with the distances between molecular centroids in the range 8.7 to 9.9 Å, calculated by the PIXEL method[21] to have intermolecular interaction energies between −56.6 and −26.5 kJ mol$^{-1}$. Intermolecular interactions, which are dominated by dispersion, take the form of stacking and other contacts between the macrocyclic pockets of the ligands. The methyl groups lie on the top and bottom surfaces of the layers, which are stacked along the *a*-direction (Fig. 2b). Three contacts are formed to the layers above and below with distances of 13.6–14.9 Å between the molecular centroids and interaction energies between −21.0 and −1.0 kJ mol$^{-1}$. The overall coordination number of each molecule is thus 12, and the structure has an underlying hexagonal close packed topology.

The unit cell parameters and the molecular volume of $Cu_2(L)$ are plotted as a function of pressure in Fig. 3. There are two distinct compression regimes, the first from ambient pressure to 3.46 GPa, and the second from 4.67 to 8.13 GPa. Up to 3.46 GPa the *a* and *b*-axes reduce by similar amounts, (4.3 and 4.9%), while the largest compression (10.1%) occurs in the *c*-axis. The principal directions of the strain tensor also align quite closely with the unit cell axes, with the largest making an angle of 8.4° with *c* and the smallest making an angle of 11.2° with *a*. The middle value lies exactly along *b* by symmetry. These data indicate that the macrocycle contacts within the layers are more compressible than the methyl–methyl contacts between the layers, even though they are stronger. For example, the stacking interaction described above shortens by almost 0.5 Å from 3.60(2) Å at ambient pressure to 3.12(3) Å at 3.46 GPa. The compressibility is much larger than for hydrogen bonds of similar energy; *e.g.* a OH···OH-bond in L-threonine (interaction energy −60 kJ mol$^{-1}$ at ambient pressure) shortens from 1.87 to 1.77 Å between 0 and 4.0 GPa.[22]

On increasing the pressure to 4.67 GPa neon becomes intercalated into the structure (Fig. 4), forming a co-crystal of stoichiometry $[Cu_2(L)]\cdot 3.5Ne$ and increasing the physical size of

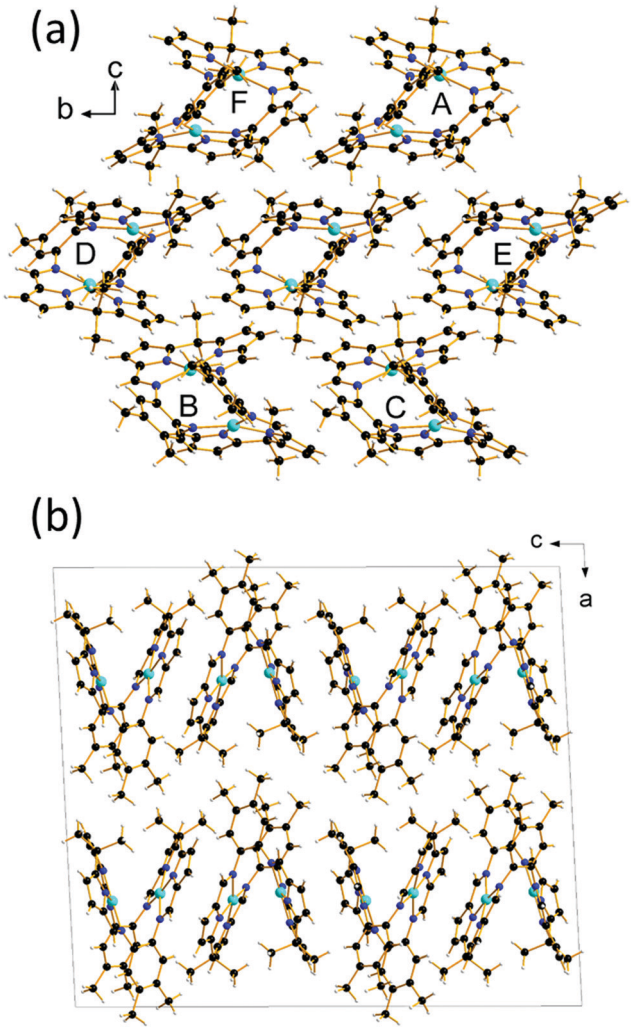


Fig. 2 (a) The six strongest molecular contacts surrounding the central reference molecule are labelled A–F and (b) layered stacking along *a*. This figure is reproduced in space-filling format in the ESI† (Fig. S1) to illustrate its non-porosity. Colour scheme: C black, H white, N blue, Cu Cyan.

the crystal (as shown in the table of contents figure and Fig. S2 in the ESI†). The pressure coincides with the freezing point of neon (4.8 GPa).[4] Freezing of neon has been implicated in prompting a phase transition in 4-hydroxycyanobenzene at 5.8 GPa, though without formation of a co-crystal.[9]

Formation of the co-crystal causes a discontinuity in the cell dimensions and volume (Fig. 3 and Table S2, ESI†). The rates of compression in the *a* and *b*-axes begin to diverge and there is a 2.0% increase in the length of the *c*-axis. The unique $\beta$ angle of the unit cell changes from 91.6° to 84.0°, but the space group remains unchanged; the value of $\beta < 90°$ ensures consistency between the structures. Beyond 4.67 GPa, the unit cell volume decreases monotonically indicating that no more neon is incorporated into the structure.

There are four Ne sites (Fig. 4). Ne1, 2 and 4 reside between the layers, forming contacts with methyl groups (see also Fig. S4, ESI†). At 4.67 GPa Ne···C distances span the range 2.70 (Ne4···C40)–3.18 Å (Ne4···C10), which imply Ne···H distances of between

 

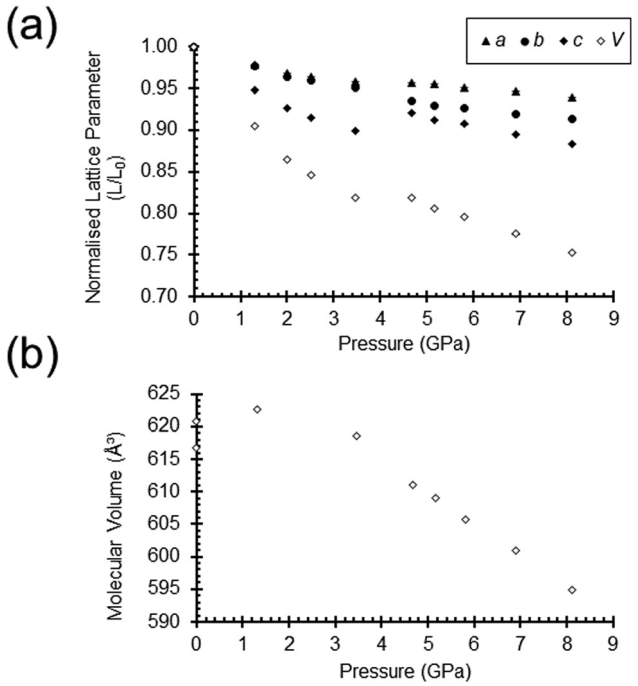


Fig. 3 (a) Normalised lattice parameters and (b) molecular volume as a function of pressure. The bulk modulus ($K_0$), obtained using a third order Birch–Murnaghan equation-of-state and the points between 0 and 3.46 GPa is 8.4(11) GPa [the pressure derivative ($K'$) = 7.4(19)].

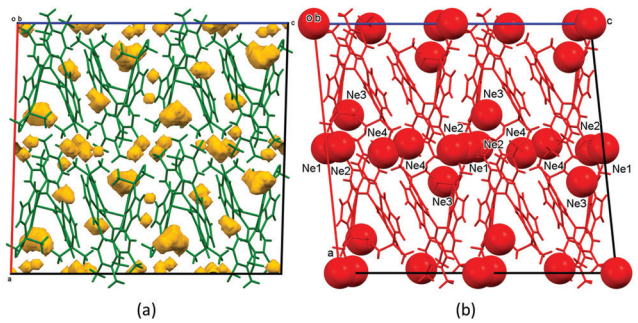


Fig. 4 (a) The structure of $Cu_2$(L) at 3.46 GPa showing void space calculated using a probe radius of 0.6 Å and a grid spacing of 0.3 Å. (b) The structure of [$Cu_2$(L)]·3.5Ne at 4.67 GPa. The Ne atoms are shown as spheres with radii equal to the van der Waals radius of Ne (1.54 Å). The view is along *b* and both images are on the same scale. An extended version of this figure is available in the ESI† (Fig. S3).

2.27 and 2.71 Å. The Ne···C distances shorten to 2.65–3.03 Å at 8.13 GPa. Ne3 is located within the layers. At 4.67 GPa it is adjacent to the cleft of the pacman ligand (Fig. S5, ESI†). The shortest Ne···N contact is made to N3 (3.03 Å at 4.67 GPa and 2.92 Å at 8.13 GPa), while the shortest Ne3···C contacts are between 2.76 Å (C24) and 2.85 Å (C22). These shorten to 2.68 and 2.75 Å at 8.13 GPa.

The crystal structure of $Cu_2$(L) at ambient pressure consists of approximately 30% empty interstitial void space. None of this volume is solvent-accessible and inspection of Fourier difference maps indicates that it contains no electron density at ambient pressure and 100 K. At 3.46 GPa the proportion of

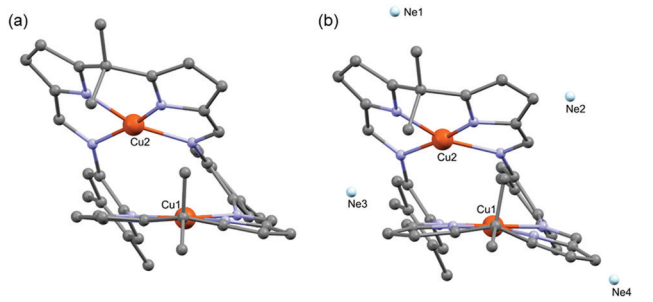


Fig. 5 (a) View of the pacman complex before the phase transition at 3.46 GPa and (b) just after the transition at 4.67 GPa showing flexing of the Pacman ligand. Ne4 not shown in (b). A side-view of the complex is also shown in Fig. S6 (ESI†).

void space reduces to 18%. The four new neon sites at 4.67 GPa are located at the same positions as the small residual voids present in the structure at 3.46 GPa (Fig. 4a). The neon atoms are shown in space-filling mode in Fig. 4b, but the sizes of the voids in Fig. 4a are not large enough to accommodate them. The non-porous crystal structure of $Cu_2$(L) thus needs to expand in order to form a co-crystal with neon.

The change in the $\beta$-angle and the lengthening of the *c*-axis means that the area of the *ac* face of the unit cell increases from 636.8 to 647.6 Å$^2$ between 3.46 and 4.67 GPa as the molecules move apart to create space for Ne1, 2 and 4. In addition the volume of the $Cu_2$(L) molecules, which had been quite constant between 0 and 3.46 GPa, also begins to decrease (Fig. 3b) as the result of a flexing of the molecular conformation (Fig. 5, Fig. S6 and Movie_1, ESI†).

The conformation of pacman complexes can be described using two parameters, a twist angle, $\phi$, which measures lateral slippage of the two macrocycle pockets, and the pacman bite angle, $\theta$ (Fig. S7, ESI†). The variation of these parameters with pressure is shown in Fig. 6.

As has been observed in the analogous chromium system ($Cr_2$(L), max. pressure = 3.0 GPa), the bite angles and metal–metal separation are both quite unresponsive to pressure up to 3.46 GPa (Fig. 6).[23] On increasing pressure to 4.67 GPa there is a sudden decrease in bite angle ($\theta$) of *ca.* 3°, which compresses

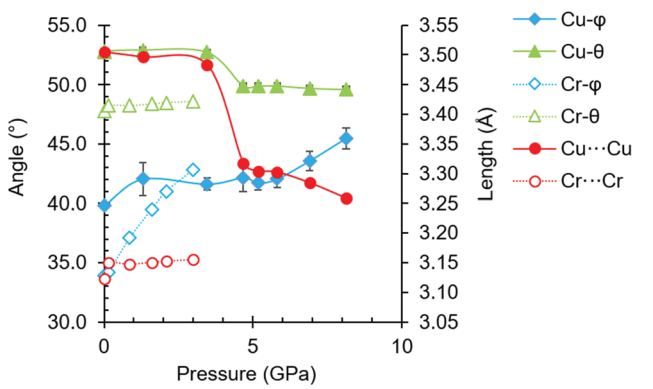


Fig. 6 Variations of the structural parameters of $Cu_2$(L) (filled markers) and $Cr_2$(L) (open markers) with pressure.

the Cu1···Cu2 separation distance abruptly from 3.4826(7) to 3.317(3) Å. The closing-up of the pacman might have been expected to reduce the space available in the region of the cleft. However, there is a simultaneous 'butterfly wing' effect in the angle between the two halves of the macrocycles, the interplanar angle changing from 7.5(2) to 20.7(7)° about Cu1 and from 25.5(2) to 34.8(7)° about Cu2 (Fig. S8 and Movie_1, ESI†). The overall effect is to enable accommodation of Ne3 in an embrace at the entrance to the cleft of the ligand. It is tempting to suggest that this may represent a pre-complexation configuration during catalysis by pacman complexes.

The bite angle and the butterfly angles of the macrocycles are relatively insensitive to further compression. The Cu separation distance continues to decrease, adopting a value of 3.258(2) Å at 8.13 GPa. The twist angle $\phi$, which in the Cr-system increased from 33.9 to 42.8° between ambient pressure and 3 GPa, in the Cu-system only begins to change above 4.67 GPa, increasing by 3° up to 8.13 GPa.

The effect of pressure on molecular solids is often rationalised in terms of compression of intermolecular void space, which naturally hinders guest inclusion. The crystal structure of $Cu_2(L)$ is, according to the usual criteria, a non-porous material under ambient conditions. Below 3.46 GPa the path of compression is similar to other molecular materials, closing up interstitial voids and shortening intermolecular contacts. The pressure-induced uptake of neon that occurs at 4.67 GPa may follow a nucleation-and-growth mechanism in which a small amount of neon is initially adsorbed, perhaps at defects, causing disruption of the crystal structure and subsequent ingress of more neon.

The conformational flexibility of the pacman complex is an essential component of the mechanism of neon inclusion. It facilitates a higher up-take than other non-porous solids such as 4-hydroxycyanobenzene and the other systems listed above, where guest inclusion requires a larger packing rearrangement leading to a phase transition. The effect is reminiscent of the gate-opening transition in the framework material ZIF-8 at 1.47 GPa which also led to an increase in guest inclusion.[5] A related effect is responsible for the low bulk moduli [6.0(7) and 4.3(3) GPa] of the P and OP polymorphs of the polymorphic material 'ROY', where conformational flexibility augments compression of intermolecular contacts to provide an additional mechanism for compression.[24,25]

This research used resources of the Advanced Light Source, which is a DOE Office of Science User Facility under contract no. DE-AC02-05CH11231. C. M. B. and beamline 12.2.2 are supported by the Consortium for Materials Properties Research in Earth Sciences (COMPRES) under NSF Cooperative Agreement EAR 1606856. N. G. is supported by EPSRC and ALS Doctoral Funding. J. R. P. was also supported by an EPSRC Doctoral Training Account studentship.

## Conflicts of interest

There are no conflicts to declare.

## References

1 R. D. L. Johnstone, M. Ieva, A. R. Lennie, H. McNab, E. Pidcock, J. Warren and S. Parsons, *CrystEngComm*, 2010, **12**, 2520–2523.
2 C. A. Hunter and R. Prohens, *CrystEngComm*, 2017, **19**, 23–26.
3 A. J. Cruz-Cabeza, S. M. Reutzel-Edens and J. Bernstein, *Chem. Soc. Rev.*, 2015, **44**, 8619–8635.
4 S. Klotz, J. C. Chervin, P. Munsch and G. Le Marchand, *J. Phys.*, 2009, **D42**, 075413.
5 S. A. Moggach, T. D. Bennett and A. K. Cheetham, *Angew. Chem., Int. Ed.*, 2009, **48**, 7087–7089.
6 J. Sotelo, C. H. Woodall, D. R. Allan, E. Gregoryanz, R. T. Howie, K. V. Kamenev, M. R. Probert, P. A. Wright and S. A. Moggach, *Angew. Chem., Int. Ed.*, 2015, **54**, 13332–13336.
7 I. E. Collings, E. Bykova, M. Bykov, S. Petitgirard, M. Hanfland, D. Paliwoda, L. Dubrovinsky and N. Dubrovinskaia, *ChemPhysChem*, 2016, **17**, 3369–3372.
8 P. A. Wood, A. A. Sarjeant, A. A. Yakovenko, S. C. Ward and C. R. Groom, *Chem. Commun.*, 2016, **52**, 10048–10051.
9 I. E. Collings and M. Hanfland, *Molecules*, 2019, **24**, 1759.
10 P. A. Guńka, K. F. Dziubek, A. Gładysiak, M. Dranka, J. Piechota, M. Hanfland, A. Katrusiak and J. Zachara, *Cryst. Growth Des.*, 2015, **15**, 3740–3745.
11 P. A. Guńka, M. Hapka, M. Hanfland, M. Dranka, G. Chałasiński and J. Zachara, *ChemPhysChem*, 2018, **19**, 857–864.
12 J. A. Sans, F. J. Manjón, C. Popescu, V. P. Cuenca-Gotor, O. Gomis, A. Muñoz, P. Rodríguez-Hernández, J. Contreras-García, J. Pellicer-Porres, A. L. J. Pereira, D. Santamaría-Pérez and A. Segura, *Phys. Rev. B: Condens. Matter Mater. Phys.*, 2016, **93**, 054102.
13 A. Arakcheeva, V. Svitlyk, E. Polini, L. Henry, D. Chernyshov, A. Sienkiewicz, G. Giriat, A. Glushkova, M. Kollar, B. Nafradi, L. Forro and E. Horvath, *Acta Crystallogr.*, 2019, **B75**, 361–370.
14 G. Givaja, M. Volpe, J. W. Leeland, M. A. Edwards, T. K. Young, S. B. Darby, S. D. Reid, A. J. Blake, C. Wilson, J. Wolowska, E. J. L. McInnes, M. Schröder and J. B. Love, *Chem. – Eur. J.*, 2007, **13**, 3707–3723.
15 A. M. J. Devoille and J. B. Love, *Dalton Trans.*, 2012, **41**, 65–72.
16 E. Askarizadeh, S. B. Yaghoob, D. M. Boghaei, A. M. Z. Slawin and J. B. Love, *Chem. Commun.*, 2010, **46**, 710–712.
17 G. Givaja, M. Volpe, M. A. Edwards, A. J. Blake, C. Wilson, M. Schröder and J. B. Love, *Angew. Chem., Int. Ed.*, 2007, **46**, 584–586.
18 M. Volpe, H. Hartnett, J. W. Leeland, K. Wills, M. Ogunshun, B. J. Duncombe, C. Wilson, A. J. Blake, J. McMaster and J. B. Love, *Inorg. Chem.*, 2009, **48**, 5195–5207.
19 J. R. Pankhurst, M. Curcio, S. Sproules, G. C. Lloyd-Jones and J. B. Love, *Inorg. Chem.*, 2018, **57**, 5915–5928.
20 M. Kunz, A. A. MacDowell, W. A. Caldwell, D. Cambie, R. S. Celestre, E. E. Domning, R. M. Duarte, A. E. Gleason, J. M. Glossinger, N. Kelez, D. W. Plate, T. Yu, J. M. Zaug, H. A. Padmore, R. Jeanloz, A. P. Alivisatos and S. M. Clark, *J. Synchrotron Radiat.*, 2005, **12**, 650–658.
21 A. Gavezzotti, *New J. Chem.*, 2011, **35**, 1360–1368.
22 N. Giordano, C. M. Beavers, K. V. Kamenev, W. G. Marshall, S. A. Moggach, S. D. Patterson, S. J. Teat, J. E. Warren, P. A. Wood and S. Parsons, *CrystEngComm*, 2019, **21**, 4444–4456.
23 C. J. Stevens, A. Prescimone, F. Tuna, E. J. L. McInnes, S. Parsons, C. A. Morrison, P. L. Arnold and J. B. Love, *Inorg. Chem.*, 2016, **55**, 214–220.
24 E. L. Harty, A. R. Ha, M. R. Warren, A. L. Thompson, D. R. Allan, A. L. Goodwin and N. P. Funnell, *Chem. Commun.*, 2015, **51**, 10608–10611.
25 N. P. Funnell, C. L. Bull, C. J. Ridley and S. Capelli, *CrystEngComm*, 2019, **21**, 4473–4483.

 